Columns formed by multiple twinning in nickel layers—An approach of grain boundary engineering by electrodeposition

Alimadadi, Hossein; da Silva Fanta, Alice Bastos; Somers, Marcel A. J.; Pantleon, Karen

Published in:
Applied Physics Letters

DOI:
10.1063/1.4816257

Publication date:
2013

Document Version
Publisher's PDF, also known as Version of record

AIP | Applied Physics Letters

Columns formed by multiple twinning in nickel layers—An approach of grain boundary engineering by electrodeposition

Hossein Alimadadi, Alice Bastos Fanta, Marcel A. J. Somers, and Karen Pantleon

Citation: Appl. Phys. Lett. **103**, 031918 (2013); doi: 10.1063/1.4816257
View online: http://dx.doi.org/10.1063/1.4816257
View Table of Contents: http://apl.aip.org/resource/1/APPLAB/v103/i3
Published by the AIP Publishing LLC.

Columns formed by multiple twinning in nickel layers—An approach of grain boundary engineering by electrodeposition

Hossein Alimadadi,[1,2] Alice Bastos Fanta,[2] Marcel A. J. Somers,[1] and Karen Pantleon[1]
[1]*Technical University of Denmark, Department of Mechanical Engineering, Produktionstorvet, building 425, DK–2800 Kongens Lyngby, Denmark*
[2]*Technical University of Denmark, Center for Electron Nanoscopy, Fysikvej, building 307, DK–2800 Kongens Lyngby, Denmark*

(Received 28 May 2013; accepted 5 July 2013; published online 19 July 2013)

Complementary microscopic and diffraction based methods revealed a peculiar microstructure of electrodeposited nickel. For the as-deposited layer, thus, without any additional treatment, multiple twinning yields a high population of $\Sigma 3^n$ boundaries, which interrupts the network of normal high angle grain boundaries. A peculiar arrangement of $\Sigma 3$ boundaries forming five-fold junctions is observed. The resulting microstructure meets the requirements for grain boundary engineering. Twinning induced effects on the crystallographic orientation of grains result in one major texture component being a $\langle 210 \rangle$ fiber axis and additional minor orientations originating from first and second generation twins of $\langle 210 \rangle$, i.e., $\langle 542 \rangle$ and $\langle 20\,2\,1 \rangle$. © *2013 AIP Publishing LLC*. [http://dx.doi.org/10.1063/1.4816257]

Grain boundaries play a significant role in the properties of polycrystalline materials.[1] Traditional materials processing has mainly aimed to control the grain size, i.e., the number of grain boundaries. More important than their number, however, is the characteristics of grain boundaries as the key for designing and controlling functional properties. Hence, materials with high fraction of special boundaries have been produced for industrial applications.[2] Low energy boundaries, and most notably $\Sigma 3$ boundaries[3] are of high importance to design grain-boundary-specific materials properties.[4,5] In this respect, materials are defined as "grain boundary engineered" if a high fraction of $\Sigma 3^n$ (n is an integer) boundaries is present and networks of normal high angle grain boundaries are interrupted.[6] Utilizing numerous nano-twin lamellae enveloped in sub-micron-sized grains, has been reported on the example of copper to bring about an improvement of the mechanical strength without reducing ductility[7] and without affecting physical properties, e.g., electrical conductivity.[8] Furthermore, such a microstructure with numerous nano-twins has a much higher thermal stability than a nanocrystalline microstructure of equal average crystallite size, but without twins.[9,10] Hence, twinning is of crucial importance for the synthesis of materials with tailored properties.

Nickel layers are characterized by high wear resistance, relatively high hardness, barrier properties, high corrosion resistance, and ease of synthesis.[11] Accordingly, a large portion of overall nickel used worldwide is in the form of thin coatings, electrodeposition being the most common metal plating process.[12] Optimizing electrodeposition conditions to tailor the grain boundaries and, thus, associated properties in nickel electrodeposits are of high interest. A Watts electrolyte, sometimes modified by additives, is the most widely used electrolyte for nickel electrodeposition.[11] Extensive studies have been carried out since the 70 s and 80 s to understand the relation between electrochemistry of the deposition process and microstructure development in the deposits of Watts-based electrolytes.[13–16] For an additive free electrolyte, it has been shown that four major fiber textures can develop: $\langle 100 \rangle$, $\langle 110 \rangle$, $\langle 211 \rangle$, and $\langle 210 \rangle$, depending on the combination of the electrolyte's pH-value and the applied current density.[13] Among them, $\langle 210 \rangle$ is the least studied; although a peculiar faceted microstructure of a $\langle 210 \rangle$ textured nickel electrodeposit is reported,[17] nickel films with a preferred $\langle 210 \rangle$ orientation are not investigated in detail until now.

The present work reports about grain boundaries and multiple twinning of a 16.5 μm-thick nickel layer with $\langle 210 \rangle$ fiber texture, electrodeposited onto an amorphous Ni-P substrate. Electrodeposition was carried out from a Watts electrolyte consisting of 300 g/dm^3 $NiSO_4 \cdot 7H_2O$, 35 g/dm^3 $NiCl_2 \cdot 6H_2O$, and 40 g/dm^3 H_3BO_3. The pH of the electrolyte was 2.5, vigorous mechanical stirring was applied and the deposition temperature was kept constant at 323 K during electrodeposition. The applied current density was 10 A/dm^2.

For quantitative crystallographic texture analysis, X-ray diffraction (XRD) pole figures of 111, 200, and 220 reflections were measured with Cu-Kα-radiation (Diffractometer D8 Discover, Bruker AXS). The azimuth angle φ was varied from 0° to 360° in steps of 5°; the sample tilt given by the pole angle ψ was varied from 0° to 75° in steps of 5°. Measured intensities were corrected for background and a Ni-powder standard was used for defocussing correction. Following,[18] the complete 3D orientation distribution function was calculated, but as the sample has a fiber texture in the direction of layer growth (normal direction, ND), the inverse pole figure in ND fully characterizes the texture in the deposit. As shown in Fig. 1(a), the major texture component is $\langle 210 \rangle$ with an orientation density of 3.8 m.r.d. (multiples of random distribution). This fiber texture is rather broad with a deviation of 9.4° around the ideal fiber axis. In addition to the major $\langle 210 \rangle$, two minor components close to $\langle 542 \rangle$ and $\langle 711 \rangle$ with orientation densities of 1.4 and 1.2 m.r.d., respectively, are identified. Calculating the twin orientation relations in FCC shows that these three orientations are related to one another by a twinning operation. The first generation of twins originating from $\langle 210 \rangle$ is either $\langle 210 \rangle$ or $\langle 542 \rangle$; and the first generation of twins from $\langle 542 \rangle$

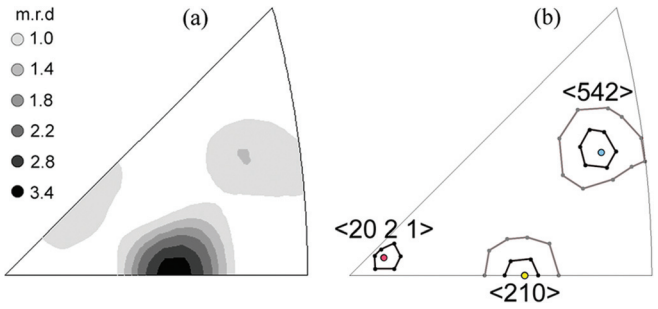

FIG. 1. Crystallographic texture analysis by XRD (a) Inverse pole figure in ND. ⟨210⟩ is the major texture component (3.8 m.r.d). ⟨542⟩ and ⟨711⟩ are minor texture components (1.4 and 1.2 m.r.d, respectively). (b) Inverse pole figure showing calculated first and second generation twins of ⟨210⟩, being ⟨542⟩ and ⟨20 2 1⟩. Twin orientations originating from an initial orientation close to ⟨210⟩ (i.e., within the measured broad maximum) are marked by black and gray regions.

are ⟨210⟩, ⟨16 10 7⟩, ⟨25 15 6⟩, and ⟨20 2 1⟩. Since the angular difference between ⟨16 10 7⟩ and ⟨542⟩ is 7.0° and that of ⟨25 15 6⟩ and ⟨542⟩ is 9.4°, and the maxima in the inverse pole figure are broad (e.g., large spread around ⟨542⟩, Fig. 1(a)), ⟨16 10 7⟩ and ⟨25 15 6⟩ cannot be resolved separately and are approximated by ⟨542⟩. Similarly, there is only a slight deviation from the calculated ⟨20 2 1⟩ orientation and the experimentally measured orientation maximum. In Fig. 1(b), ⟨210⟩, ⟨542⟩, and ⟨20 2 1⟩ are shown by yellow, light blue, and light red dots, respectively. Taking into account the broadness of the ⟨210⟩ fiber component, twinning operations of ⟨210⟩ → ⟨542⟩ and ⟨542⟩ → ⟨20 2 1⟩ are also calculated for other orientations close to the ideal fiber axis (black and gray lines around the ⟨210⟩ in Fig. 1(b)). It is noted that further possible twinning such as ⟨210⟩ → ⟨210⟩, ⟨542⟩ → ⟨210⟩, etc. are not considered in the calculations. Nevertheless, despite the apparent deviation, there is a satisfactory agreement between the expected twin components and the measured textures. Hence, the global XRD analysis, i.e., averaging over about the whole layer thickness, strongly suggests that up to the second generation of twins originating from the major texture component are present in the microstructure.

To investigate the local texture and examine the character of the grain boundaries, electron backscatter diffraction (EBSD) and ion channeling imaging (ICI) were performed in a FEI Helios NanoLab^{TM} 600, equipped with an EDAX-TSL EBSD system and a Hikari camera. The EBSD measurement was performed in a hexagonal grid with an electron probe current of 5.5 nA at an acceleration voltage of 12 kV, with step size of 25 nm. The cleaning procedure of the measured data was applied using OIM 5^{TM} as follows: (i) grain confidence index standardization, (ii) single iteration grain dilation (in both cases, a grain was defined as a region consisting of at least four connected points with misorientations of less than 5°), (iii) all the data points with confidence index below 0.1 were disregarded. The ICI investigation was performed using Ga^+ ions with an energy of 30 keV and ion density of 2.6 C/m^2 on the same location, where the orientation map was acquired beforehand for supplementary characterization at higher resolution.[19] Images covering the whole thickness of the deposit are shown in Fig. 2. Based on the ion channeling image (Fig. 2(a)), the grain size is estimated to be below 50 nm in the near-interface region (the first 1 μm) of the layer. Consequently, in this region no reliable information was obtained with EBSD for the current conditions, as is reflected by the ragged appearance and the relatively many non-indexed pixels (white regions in the orientation map, Fig. 2(b)). At a thickness of 1 μm, relatively large grains with characteristic straight boundaries have developed. With increasing distance from the substrate, the grain size increases, but the same characteristic straight boundaries remain. The orientation map in Fig. 2(b) shows that most of those straight boundaries are Σ3 boundaries (shown in black). Furthermore, it shows that the microstructure is composed of ⟨210⟩ oriented columns (yellow to yellowish green) and that the ⟨210⟩ oriented columns consist of a chain of ⟨210⟩ oriented grains, which are separated by Σ3 boundaries and, thus, must be a result of repeated and multiple twinning.

In Fig. 3, one column of ⟨210⟩ oriented grains and its neighboring grains is highlighted and shown as an orientation map (Fig. 3(a)). It is evident from Fig. 3(a) that a ⟨210⟩ oriented grain is twinned into another ⟨210⟩ oriented grain, which at its turn twins into another ⟨210⟩ grain. Accordingly, a column dominated by ⟨210⟩ oriented grains is the result of ⟨210⟩ → ⟨210⟩ twinning. Clearly ⟨542⟩ oriented grains (in light blue/purple color) are bounding the ⟨210⟩ oriented

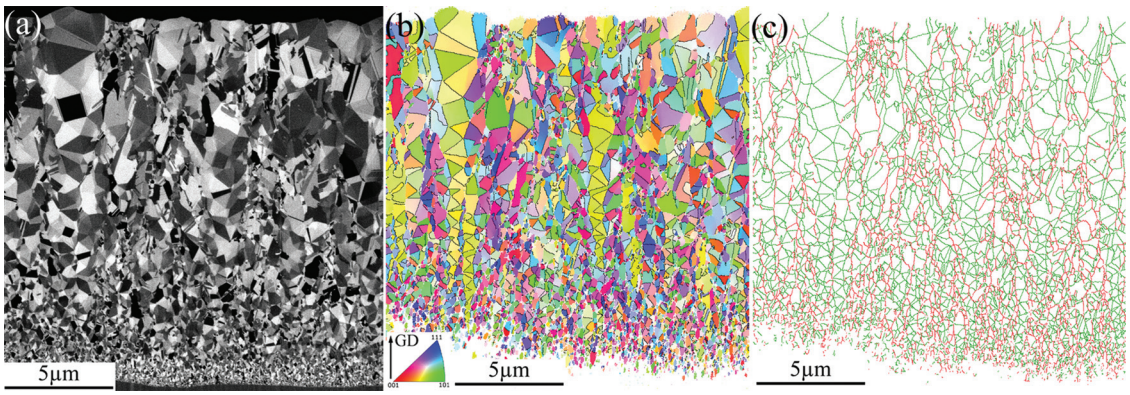

FIG. 2. Microstructure of the cross section of the layer from the layer/substrate interface to the surface (in all figures the same location is shown). (a) Ion channeling image. Note that many boundaries are straight lines. (b) Orientation map, color coded in relation with the electrodeposit's growth direction (GD) shown by an arrow in the legend; Σ3 boundaries are shown in black; (c) High angle grain boundary network, $\Sigma 3^n$ (n = 1,2,3) boundaries are shown in green and all other high angle grain boundaries in red.

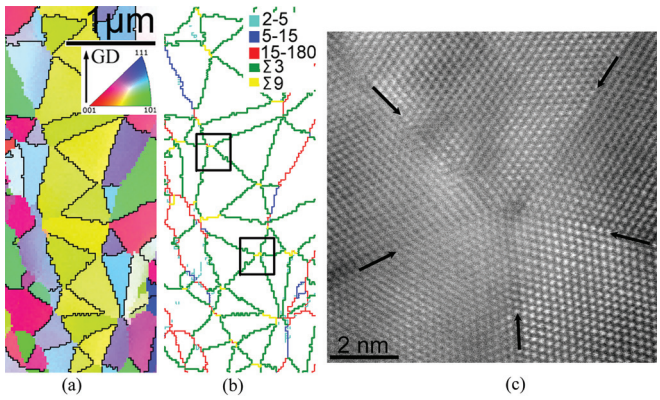

FIG. 3. (a) Orientation map, color coded in relation with the electrodeposit's GD shown by an arrow; Σ3 boundaries are shown in black (other boundaries are not marked). (b) Grain boundary network; normal high angle grain boundaries are in red, Σ3 in green, Σ9 in yellow, boundaries with misorientation 2°–5° in light blue and 5°–15° in dark blue. Black squares show selected regions with five-fold junction. (c) TEM micrograph, showing a five-fold junction, five boundaries marked by arrows actually meet in a single point.

column and are separated from the ⟨210⟩ grains by a Σ3 boundary. Moreover, it is observed that ⟨542⟩ oriented grains either have a ⟨210⟩ or another ⟨542⟩ oriented grain as their direct neighbor. Thus, it appears that ⟨542⟩ grains do not form independently but rather are the result of twinning of a ⟨210⟩ or another ⟨542⟩ grain (⟨210⟩ → ⟨542⟩ → ⟨542⟩). The ⟨20 2 1⟩ grains (in reddish colors) also have a ⟨542⟩ oriented grain as a neighbor, and a Σ3 boundary separates the two grains. This shows that ⟨20 2 1⟩ is also the result of twinning, ⟨210⟩ → ⟨542⟩ → ⟨20 2 1⟩. Interestingly, Fig. 3(a) reveals Σ3 boundaries between ⟨20 2 1⟩ oriented grains (in reddish color) and ⟨551⟩ oriented grain (in dark green color). These two orientations are also in twin relation. This indicates that even the third generation of twins of ⟨210⟩ grains is present locally. In the texture investigation with XRD (Fig. 1(a)), the population of ⟨551⟩ oriented grains does not exceed random distribution. Accordingly, the population of third generation twins is not of significance in this material.

Since multiple twinning is evidently has occurred in the studied material, a high fraction of $\Sigma 3^n$ boundaries is expected in the microstructure.[20,21] Averaging the length fraction of $\Sigma 3^n$ boundaries over the layer thickness, 54.3% of all high angle grain boundaries are in fact of $\Sigma 3^n$ character. Importantly, for larger distances from the film/substrate interface the length fraction of $\Sigma 3^n$ boundaries is higher than the average, e.g., for the upper 12 μm of the layer it is above 60%. In addition, the network of normal high angle grain boundaries is interrupted; i.e., there is no passage of normal high angle grain boundaries from the substrate to the surface (see Fig. 2(c)). Thus, the two requirements of grain boundary engineered material, i.e., (i) high population of $\Sigma 3^n$ boundaries and (ii) interrupted networks of normal high angle grain boundaries[6] are satisfied for the 16.5 μm-thick electrodeposited nickel layer. Notably, the grain boundary engineered microstructure is achieved in the as-deposited state and, in contrast to iterative thermomechanical treatments,[5] no further post-deposition treatment is required to achieve such a high population of special boundaries in the present electrodeposit. It is noted that by increase of film thickness, population of $\Sigma 3^n$ boundaries and grain size increases. The former is beneficial for enhanced grain boundary specific properties, whereas the latter is deteriorating mechanical strength. Hence, thickness should be optimized as a trade of between the two for different applications. In addition to thickness, careful selection of electrodeposition conditions can significantly influence multiple twinning and, hence, the resulting microstructure. The origin of multiple twinning is not completely understood yet. For the applied deposition conditions, i.e., low pH and high current density, hydrogen evolution is favored.[13] Thus, it is suggested that the evolution of H_2, at the cathode/electrolyte interface plays a role.

A peculiar observation is that in the regions with abundant Σ3 boundaries a five-fold junction of straight boundaries occurs. In Fig. 3(b), a network of grain boundaries in such a region is shown and two of the five-fold junctions are marked by the black rectangles. EBSD analysis identified the occurrence of Σ9 boundaries, with length of 2–3 pixels (50–75 nm) in the center of a five-fold junction of Σ3 boundaries. Altogether five Σ3 boundaries meeting in a single point would span a total angle of 352.6°, only 7.4° from a full rotation. Then, it might be suggested that the closing angle of 7.4° is compensated by the occurrence of a small Σ9 boundary, so that no actual five-fold junction occurs. However, TEM investigations in a Titan 80–300 filed emission TEM, from FEI operated at 300 KV, in HAADF-STEM mode, show that the five boundaries actually do meet in the center of five-fold junctions, see Fig. 3(c). Hence, the Σ9 boundaries identified in the orientation map at the center of a five-fold junction are merely an artifact, caused by the choice of a hexagonal grid for measurement of the orientation map (up to 3 boundaries can meet in one point in such a grid). Thorough analysis of Σ9 boundaries as well as the thermal stability of the layers consisting of numerous and multiple twins are of high importance[22] and will be addressed elsewhere.

Summarizing, it was demonstrated by combining XRD texture measurements and local orientation analysis by EBSD that electrodeposition of nickel from a highly acidic Watts electrolyte and high current density, results in multiple twinning of ⟨210⟩ oriented grains. This yields the development of peculiar ⟨210⟩ columns with sequences of twins within individual columns and, thus, a high number of Σ3 boundaries separating the grains forming these columns. Finally, by careful selection of electrodeposition conditions, grain boundary engineered material can be achieved.

The authors acknowledge the Danish Research Council for Technology and Production Sciences (Grant No. 274-07-0492) for financial support. The authors thank Dr. Takeshi Kasama, DTU Cen, for cooperation on transmission electron microscopy. The A. P. Møller and Chastine Mc-Kinney Møller Foundation is gratefully acknowledged for their contribution toward the establishment of the Center for Electron Nanoscopy in the Technical University of Denmark.

[1]T. Watanabe, Mater. Sci. Eng., A **166**, 11 (1993).
[2]G. Palumbo, E. Lehockey, and P. Lin, JOM **50**, 40 (1998).
[3]G. Hasson, J. Y. Boos, I. Herbeuval, M. Biscondi, and C. Goux, Surf. Sci. **31**, 115 (1972).
[4]X. Fang, K. Zhang, H. Guo, W. Wang, and B. Zhou, Mater. Sci. Eng., A **487**, 7 (2008).

[5]V. Randle, Acta Mater. **52**, 4067 (2004).
[6]C. A. Schuh, M. Kumar, and W. E. King, Acta Mater. **51**, 687 (2003).
[7]L. Lu, X. Chen, X. Huang, and K. Lu, Science **323**, 607 (2009).
[8]L. Lu, Y. Shen, X. Chen, L. Qian, and K. Lu, Science **304**, 422 (2004).
[9]X. Zhang, O. Anderoglu, R. G. Hoagland, and A. Misra, JOM **60**, 75 (2008).
[10]Y. Zhao, T. A. Furnish, M. E. Kassner, and A. M. Hodge, J. Mater. Res. **27**, 3049 (2012).
[11]G. A. DiBari, Met. Finish. **99**, 270 (2001).
[12]J. K. Dennis and T. E. Such, *Nickel and Chromium Plating* (Woodhead Publishing, Cambridge, 1993), p. 1.
[13]J. Amblard, I. Epelboin, M. Froment, and G. Maurin, J. Appl. Electrochem. **9**, 233 (1979).
[14]J. P. Hoare, J. Electrochem. Soc. **133**, 2491 (1986).
[15]I. Gündiler and L. E. Murr, Thin Solid Films **37**, 387 (1976).
[16]V. Velinov, S. Vitkova, and N. Pangarov, Surf. Technol. **6**, 19 (1977).
[17]J. Amblard, G. Maurin, D. Mercier, and N. Spyrellis, Scr. Metall. **16**, 579 (1982).
[18]H. J. Bunge and P. R. Morris, *Texture Analysis in Materials Science: Mathematical Methods* (Butterworths, London, 1982).
[19]H. Alimadadi, A. B. Fanta, and K. Pantleon, J. Microsc. **249**, 111 (2013).
[20]V. Y. Gertsman and C. H. Henager, Interface Sci. **11**, 403 (2003).
[21]C. Cayron, Acta Crystallogr., Sect. A: Found. Crystallogr. **63**, 11 (2007).
[22]V. Randle, M. Coleman, and M. Waterton, Metall. Mater. Trans. A **42**, 582 (2011).